




# Multifunctional molecules of surfactant to support enhanced efficiency and stability for perovskite solar cells

Qintao Wang<sup>1</sup>, Haimin Li<sup>1\*</sup> , Jia Zhuang<sup>1</sup>, Heng Guo<sup>1</sup>, Xingchong Liu<sup>1</sup>, Zhongli Guo<sup>1</sup>, Xiaoli Gong<sup>1</sup>, and Haoyue Li<sup>1</sup>

<sup>1</sup> School of New Energy and Materials, Southwest Petroleum University, Chengdu 610500, Sichuan, China

Received: 22 February 2020

Accepted: 5 July 2020

Published online:

20 July 2020

© Springer Science+Business Media, LLC, part of Springer Nature 2020

## ABSTRACT

As the darling of new era, perovskite solar cells (PSCs) have drawn extensive attention because of their tremendous commercial potentials. However, many different types of defects are easily formed during the fabrication process of perovskite films, such as cation and anion vacancy, under-coordinate metal ions, humidity erosion and so on, which are detrimental to the efficiency and long-term stability of the devices. To decrease the charge trap density and improve the moisture resistance of the perovskite film, here, we introduce a multifunctional surfactant, cetyl trimethyl ammonium bromide (CTAB), into perovskite precursor solution to both passivate the two types of ionic vacancies and also enhance the humidity resistance. Benefiting from Br and quaternary cetyl tertiary ammonium cations filled up on X- and A-sites, fluorescence spectrum revealed that moderate CTAB doped perovskite films showed decreased defects and inhibited carrier recombination. Consequently, ternary cation perovskite solar cells with optimized CTAB additives deliver an enhanced champion power conversion efficiency (PCE) of 20.54% and outstanding long-range stability with 94.3% of the initial efficiency after 2000 h without encapsulation in N<sub>2</sub> atmosphere.

## Introduction

Organic–inorganic hybrid perovskite solar cells (PSCs) as a family member of new-generation thin film solar cells are placed great expectations. Owing to their remarkable optical and electrical properties, such as large optical absorption coefficient [1],

tunable bandgap [2], high carrier mobility and long diffusion length [3, 4], the power conversion efficiency (PCE) of PSCs has mushroom increased from 3.8% to more than 25% within a decade [5, 6]. Although impressive progress has been made, the commercialization application of PSCs is still hampered by many issues. The solution-based deposition methods in PSCs manufacturing are cost-effective

Address correspondence to E-mail: lucialeee@126.com

and large-scale available. However, precisely because of their low formation energy [7, 8], a large number of trap states easily induced by cracks or crystal defects at the grain boundaries (GBs) and surfaces of the perovskite film promote nonradiative recombination that causes decreased charge carrier lifetime, undesired ion migration, sequentially detrimental to the efficiency and stability of the PSCs [9–13].

Recently, defects passivation as one of the major valid strategies for suppressing the charge recombination and increasing the carrier lifetime in perovskite film has been extensively studied. By adding either organic halide salts, inorganic acids, polymers, hydrophobic and two-dimensional (2D) small molecules into the perovskite precursor solution or anti-solvent, the enlarged grain size and improved morphology of polycrystalline film can be easily obtained [14–21]. For example, Liu and co-workers added a tiny amount of N,1-diiodoformamidine (DIFA) in perovskite precursor solution to achieve smooth perovskite film with enlarged grain size up to nearly 3  $\mu\text{m}$ , resulting in significantly reduced GBs and trap densities, with the enhanced PCE of 21.22% [22]. Wu et al. introduced 3-phenyl-2-propen-1-amine iodide (PPEAI) into the anti-solvent (CB) to modify the interfacial characteristic of perovskite films via interfacial stitching effect [23]. So far, many small molecules or polymer additives as a passivation agent reducing the defects and improving the photovoltaic properties of PSCs have been reported by other groups [24–26]. Nevertheless, profoundly understanding the mechanism of defect passivation, ingeniously design multifunctional molecules that can simultaneously passivate various defects in perovskite film are still a huge challenge for academics all of the world.

Herein, a surfactant, cetyl trimethyl ammonium bromide (CTAB), containing quaternary cetyl tertiary ammonium cation, halogen bromide and long alkyl chain was tentatively introduced into the perovskite precursor solution. It is attested that the perovskite devices with a crumb of CTAB doped could effectively passivate the cation and anion defects, reduce the charge recombination and elongate the carrier lifetime. The perovskite morphology exhibited increased grain size, reduced cracks and roughness, resulting in the improved film quality that is helpful to promote carrier extraction and transportation. The optimized CTAB-doped  $\text{Cs}_{0.05}(\text{FA}_{0.85}\text{MA}_{0.1})\text{Pb}(\text{I}_{0.85}\text{Br}_{0.15})_3$  planar-based perovskite solar cells show

significantly increased short-circuit current density ( $J_{\text{sc}}$ , from 22.7 to 23.3  $\text{mA}/\text{cm}^2$ ) and fill factor (FF, from 73 to 76%), which are profit from the increased light absorption and decreased defect states. Correspondingly, the champion solar cell shows a  $J_{\text{sc}}$  of 23.32  $\text{mA}/\text{cm}^2$ , a  $V_{\text{oc}}$  of 1.114V and a FF of 79.1% and obtains a PCE of 20.54%, which is much higher than the control ones (PCE = 18.13%). Moreover, the improved hydrophobicity effectively obstructs the erosion of water and reduces the degradation under ambient pressure; thereby, the stability of the PSCs based on CTAB doped is effectively improved as well, demonstrating 94.3% of initial efficiency after 2000 h without encapsulation in  $\text{N}_2$  atmosphere.

## Materials and methods

### Materials

FTO glass substrates were purchased from Ying kou you xuan Trade Co., Ltd. Formamidinium iodide (FAI), lead iodide ( $\text{PbI}_2$ ), cesium iodide (CsI), lead bromide ( $\text{PbBr}_2$ ), methyl ammonium bromide (MABr) and 2,2',7,7'-tetrakis (N,N-dimethoxyphenylamine)-9,9'-spirobifluorene (Spiro-OMeTAD) were purchased from Xi'an Polymer Light Technology Corp. N,N-dimethylformamide (DMF, 99.8%) and dimethyl sulfoxide (DMSO) were obtained from Sigma. Tin (IV) oxide and 15% in  $\text{H}_2\text{O}$  colloidal dispersion liquid were purchased from Alfa. All solvents and raw materials were obtained from commercial sources and used without further purification.

### Device fabrication

ITO glass substrates were ultrasonic cleaned by ethanol, acetone, deionized water and isopropanol, successively, each step lasted for 20 min and finally dried with nitrogen gas. The organic residues on the surface of the substrates were treated with UVO for 20 min.  $\text{SnO}_2$  electron transport layer (ETL) was prepared by spinning  $\text{SnO}_2$  solution (tin oxide, 15% in  $\text{H}_2\text{O}$  colloidal dispersion liquid, diluted by deionized water with a volume ratio of 1:5) at 3000 rpm for 30 s and then baked on a hot plate at 150  $^\circ\text{C}$  for 30 min. After cooling down to room temperature,  $\text{Cs}_{0.05}(\text{FA}_{0.85}\text{MA}_{0.1})\text{Pb}(\text{I}_{0.85}\text{Br}_{0.15})_3$  perovskite film was deposited by spin coating the perovskite precursor

solution with or without CTAB (FAI 1 M, MABr 0.2 M,  $\text{PbI}_2$  0.2 M,  $\text{PbBr}_2$  0.2 M) were dissolved in dimethylformamide (DMF) and dimethyl sulfoxide (DMSO) (v/v, 4:1). 1.5 M solution of CsI was added into the above mixed solution. CTAB powder was doped into the above precursor solution with different concentrations (molar ratio, 0, 1%, 2%, 3%). Perovskite solution was coated on the ETL and spun with a speed of 1000 rpm for 10 s and 5000 rpm for 30 s; 120  $\mu\text{L}$  of chlorobenzene (CB) was dropped on the spinning substrate 10 s before the ending of the program. The substrates were then annealed at 100 °C for 45 min to form the perovskite phases. After annealing, HTL was spin-coated at 3000 rpm for 30 s. The HTL was prepared by dissolving 72.3 mg Spiro-OMeTAD in 1 mL CB doped with 17.5  $\mu\text{L}$  bis(trifluoromethylsulfonyl) imide lithium salt solution (520 mg Li-TFSI in 1 mL acetonitrile) and 28.8  $\mu\text{L}$  4-tert-butylpyridine (TBP). Finally, about 80 nm Ag electrode was deposited on the Spiro-OMeTAD film by magnetron sputtering. The devices active area is determined by a shadow mask to be 0.08  $\text{cm}^2$ .

### Characterization and measurements

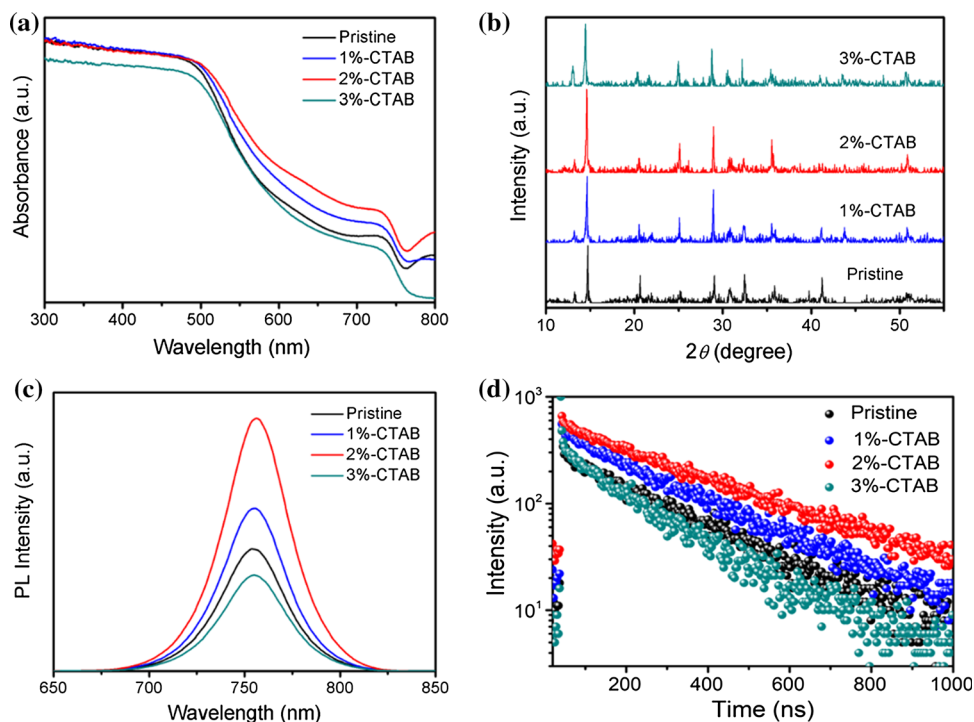
The absorption characteristics of perovskite films were characterized using ultraviolet–visible (UV–Vis) spectrophotometry (UV-2600). Contact angle was measured by an automatic contact angle tester (OCA25, TBU95, THX-05). The morphologies of surface and cross-section images of the perovskite films were obtained by a field emission scanning electron microscopy (FEI Quanta 650 FEG). Steady and time-resolved photoluminescence spectroscopy (PL and TRPL) was tested by a fluorescence spectrometer (FLS 1000, Edinburgh Instruments). The PL spectrum was measured with a 468 nm excitation wavelength. The TRPL decay was recorded with the excitation wavelength at 405 nm. XRD results were carried out by using a DX-2700B X-ray diffractometer. AFM was measured by KEYSIGHT Technologies 7500. The current density–voltage (J–V) curve of the PSCs was obtained by using a electrochemical workstation (CHI660D) under an illumination of AM 1.5G solar simulator (Zolix SS150) with a reverse scan from 1.2 to – 0.2V and a forward scan from 0.2 to 1.2V. Electrochemical workstation was also used to perform the impedance spectroscopy under the  $V_{\text{mpp}}$  in the dark. EQE was recorded using an incident photo-to-

electron conversion efficiency (IPCE) system (PVE300, Bentham, Inc.), which is calibrated by a reference silicon cell before testing.

### Results and discussion

To understand the change in light absorption, we first performed the absorption spectra of perovskite films without and with different concentrations of CTAB doping. As Fig. 1a shows, there has a distinct absorption increasing from 500 to 800 nm wavelength in 1% and 2% CTAB-added samples. The increased absorption is probably caused by the improved morphology and crystallinity of the active layer after a small quantity of CTAB adding. However, the thickness of perovskite film did not change obviously before and after the addition of CTAB, as shown in Figures S1 and S2, Supporting Information. In addition, we also noticed that the absorbance around 800 nm is nonzero, and this is mainly due to other light absorption process, such as exciton absorption, impurity absorption and free carrier absorption, for the incident light wavelength is larger than the intrinsic absorption edge. Then, we investigated the compositional changes and crystallinity of these perovskite films by X-ray diffraction (XRD). As shown in Fig. 1b, there were no additional new peaks observed after different degrees of CTAB doping (Figure S3, Supporting Information, shows the XRD patterns of the CTAB). This means that moderate CTAB adding did not introduce the impurity phase and change the crystal structure of perovskite. We also noticed that there is a hill located at around  $13.2^\circ$ , which represents the characteristic peak of  $\text{PbI}_2$  [27]. Previous research reported that the proper amount of  $\text{PbI}_2$  releasing would be beneficial for passivating the grain boundary (GB) defects on perovskite surface [28]. Thus, a handful of  $\text{PbI}_2$  peaks remaining in this paper helps to obtain the high efficiency of PSCs. Moreover, the most essential characteristic peak at  $\sim 14.7^\circ$  represents the (110) lattice plane of perovskite film [29]. It is worth noting that the peak intensity of (110) lattice plane changes as the amount of CTAB increases. In the meanwhile, the 2% CTAB-added perovskite film shows the strongest intensity of all perovskite characteristics peaks, demonstrating the increased crystallinity. However, there shows significantly increased  $\text{PbI}_2$  peak and decreased (110) peak when CTAB is further increased to 3%, and this

**Figure 1** **a** UV–Vis absorption spectra, **b** XRD patterns, **c** steady-state PL spectra and **d** TRPL spectra of the pristine and different concentrations of CTAB-doped perovskite films deposited on ITO substrate.



might be because the surplus CTAB doping inhibited the conversion of  $\text{PbI}_2$  to perovskite phase and ultimately caused the efficiency deficit of the devices. Beyond that, we also found that as the adding amount of CTAB increases, the (110) characteristic peak of perovskite shifted to low diffraction angle ceaselessly (Figure S4, Supporting Information). The shifted XRD peaks reflect the change of chemical composition [30], which indicates that the quaternary ammonium (QA) cation and  $\text{Br}^-$  ions in CTAB can partially replace or fill the vacancy at the A-site or X-site and result in the lattice expansion [15].

As we all know, there was a close relationship between carrier recombination and defect concentration in perovskite film [31], which drastically affects the charge carrier extraction and transportation. To investigate the charge carrier dynamics within the devices, we measured the steady-state photoluminescence (PL) and time-resolved photoluminescence (TRPL) of the perovskite film without any charge transportation layers (CTLs) deposition. Defect passivation can reduce the trap-state density in perovskite film and thus manifest the increased PL intensity. Although the increased absorption contributes to the enhancement of the PL intensity, however, the absorbance of 2% CTAB-doped perovskite film is just a little bit higher than other films at excitation wavelength of 468 nm, which could not

induce the PL intensity to more than double of pristine film, as Fig. 1a, c shows. Here, the sharp increase in PL intensity is mainly due to the enhanced film crystallinity and reduced trap-state density. Correspondingly, the average lifetime values of the CTAB-doped sample obtained by time-resolved PL spectroscopy give prolonged activity (245.02 ns for 1% CTAB, 302.43 ns for 2% CTAB) than that of the pristine perovskite film (227.87 ns). The calculation formula and specific parameters are listed in Supporting Information, Table S1. The results of PL and TRPL collectively confirm the inhibition function in trap states and carrier recombination induced by 2% CTAB introduction. Furthermore, it has also been noticed that the PL intensity and carrier lifetime have a plunge after 3% CTAB adding, which is even worse than that of the control group. This may happen because the superfluous CTAB reduced the crystallinity and photovoltaic properties of the perovskite films by reason of the insulation nature of the long alkyl chain, which is consistent with the XRD results.

Figure 2a–d shows the surface scanning electron microscopy (SEM) of the perovskite film with different CTAB doping. Compared with the pristine perovskite film, the 2% CTAB additive perovskite film exhibits more dense morphology with fewer holes and cracks. The grain size distribution of the different perovskite composition is depicted in



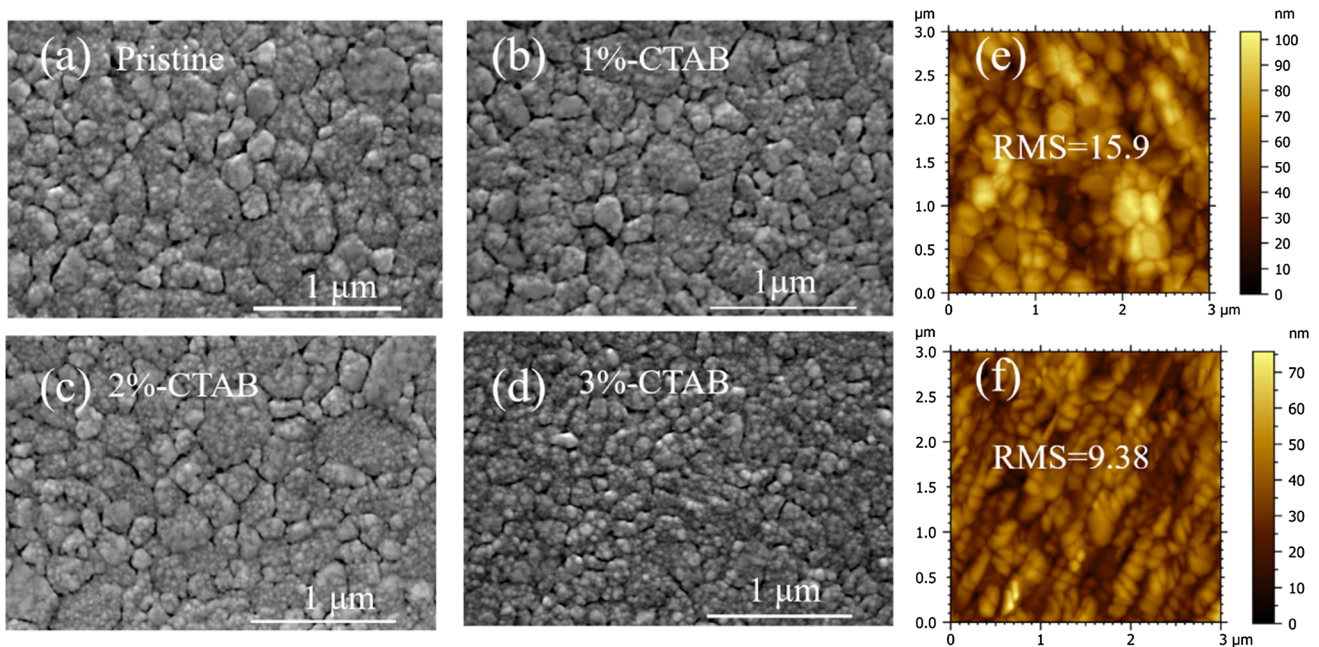


**Figure 2** Top-view SEM images of the perovskite films for **a** pristine, **b** 1% CTAB doped, **c** 2% CTAB doped, **d** 3% CTAB doped. AFM images of the perovskite films with **e** pristine and **f** 2% CTAB additive.

Figure S6, Supporting Information. Apparently, perovskite precursor solution with 2% CTAB doping is conducive to decrease the defects and increase the crystallinity and grain size of the deposited film, which are helpful for reducing the leakage current and improving the performance of the devices. Surprisingly, the perovskite grain with 3% CTAB doped shows a disorderly arrangement and reduced size. Furthermore, a good deal of flakes can be clearly observed, which might be the remanent CTAB and  $\text{PbI}_2$  aggregated around perovskite grains. These flakes wrapped on perovskite film will suppress the grain growth and impede the carrier transport between activity layer and CTLs. Atomic force microscopy (AFM) was further used to evaluate the roughness of the different perovskite films. As shown in Fig. 2e, f, the root-mean-square (RMS) values of the perovskite film reduced from initial 15.9–9.38 nm after 2% CTAB adding. The flatter topography and larger grain size of the perovskite film with 2% CTAB additive would contribute to carrier transportation and suppress the charge recombination, resulting an improvement in the photovoltaic performance of the PSCs [16, 32].

Considering the advantage of the high efficiency and well-crystallized ternary cation perovskite, the planar PSCs based on the  $\text{Cs}_{0.05}(\text{FA}_{0.85}\text{MA}_{0.1})\text{Pb}(\text{I}_{0.85}\text{Br}_{0.15})_3$  perovskite absorber layer were fabricated,

and the complete device structure is depicted in Fig. 3a. The best current density–voltage ( $J$ – $V$ ) characteristics of the PSCs with different concentrations of CTAB were tested under AM 1.5G illumination with one sunlight intensity ( $100 \text{ mW}/\text{cm}^2$ ) (Fig. 3b, Table 1). We can see that the pristine PSC device has an open-circuit voltage ( $V_{oc}$ ) of 1.072V, a short-circuit current density ( $J_{sc}$ ) of  $22.76 \text{ mA}/\text{cm}^2$  and a fill factor (FF) of 74.3% yielding a PCE of 18.13%. The sample with 2% CTAB additives exhibited overall improvement in  $V_{oc}$ ,  $J_{sc}$ , FF and obtained a  $V_{oc}$  of 1.114 V,  $J_{sc}$  of  $23.32 \text{ mA}/\text{cm}^2$ , FF of 79.1%, with a champion efficiency of 20.54%. The increased  $V_{oc}$  and FF can be explained by the reduction of defects, and the increased  $J_{sc}$  can be attributed to the improved perovskite film and light absorption, resulting the PCE improvement of the devices. However, after 3% CTAB doping in  $\text{Cs}_{0.05}(\text{FA}_{0.85}\text{MA}_{0.1})\text{Pb}(\text{I}_{0.85}\text{Br}_{0.15})_3$ , a terrible phenomenon showed that the performance of the device decreased sharply. This was probably because the residual CTAB in perovskite film introduced more defects and caused graver carrier recombination, which vastly damages the photovoltaic performance of the device. Hysteresis phenomenon is familiar in PSCs as the reason of that the surface defects and ion migration trigger the interfacial capacitance resistance [33, 34]. Based on this, the hysteresis index (HI) was introduced to evaluate

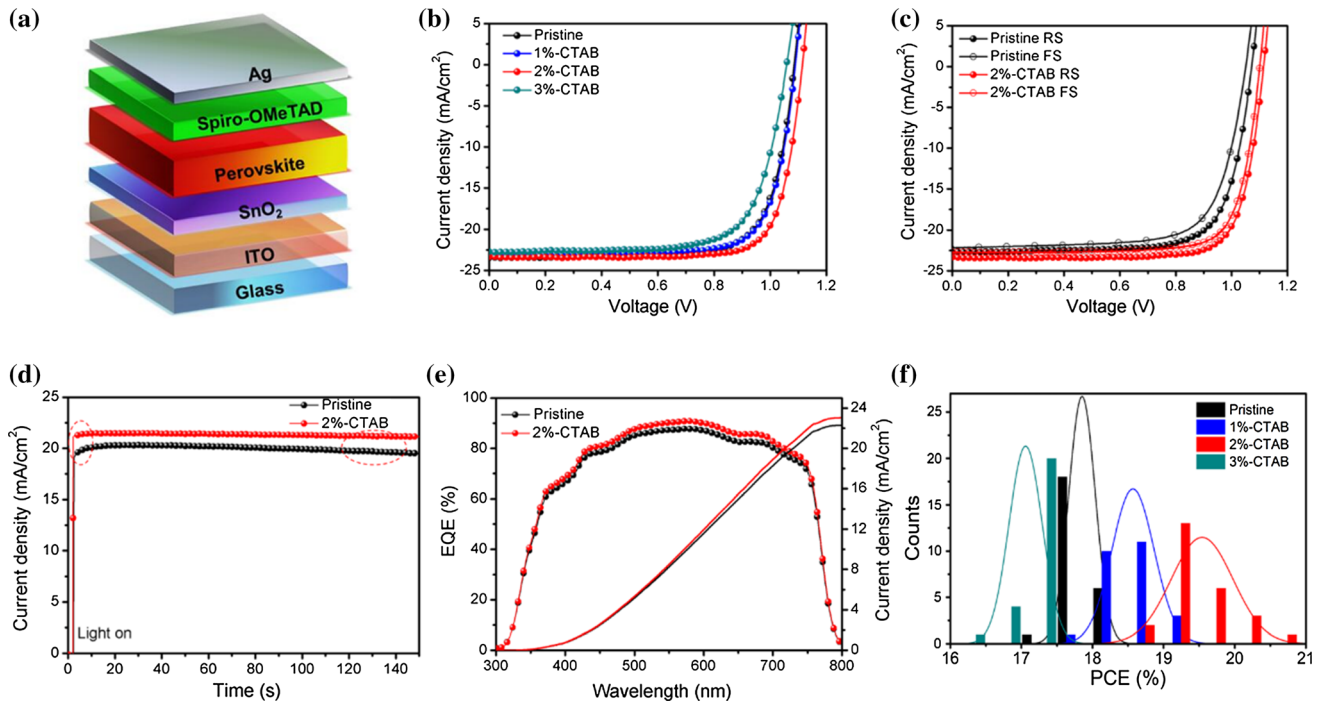


**Figure 3** **a** The diagram of the completed device structure. **b**  $J$ – $V$  curves of the best PSCs for pristine and different concentrations of doped CTAB. **c** Hysteresis behavior of the PSCs without and with CTAB additives tested under reverse and forward scan direction.

**d** Steady-state output of current density of the PSCs without and with CTAB additives. **e** EQE spectra of PSCs without and with CTAB additives and corresponding integrated  $J_{sc}$  of the devices. **f** The histogram of PCE distribution.

**Table 1** The photovoltaic parameters of different PSCs

Sample	$V_{oc}$ (V)	$J_{sc}$ (mA/cm <sup>2</sup> )	FF (%)	PCE (%)
Pristine	1.072	22.76	74.3	18.13
1% CTAB	1.090	23.35	75.1	19.18
2% CTAB	1.114	23.32	79.1	20.54
3% CTAB	1.059	22.71	72.4	17.41

the degree of hysteresis, which was measured from different scan directions and expressed as the following equation [35]:

$$\text{Hysteresis Index (HI)} = \frac{\text{PCE}_{\text{reverse}} - \text{PCE}_{\text{forward}}}{\text{PCE}_{\text{reverse}}}$$

In this paper, the device without the CTAB additive showed a PCE of 18.13% for the reverse scan and 16.83% for the forward scan, giving a HI of 7.17%. Gratifyingly, the HI of the 2% CTAB-doped cell decreased to 4.62% (20.54% for RS, 19.59% for FS), which is much weaker than the control group (Fig. 3c). It seems that the alleviative hysteresis after CTAB adding may, in greater degree, benefit from the decreased defects and improved carrier extraction

[29, 36]. Figure 3d presents the stability of the photocurrent, which is measured under the maximum power point (MPP) of the devices which measure with and without CTAB introduced. It can be seen that the photocurrent of the CTAB-added device was rapidly stabilized at 21.15 mA/cm<sup>2</sup> when the light was turned on. In response, the control device shows a relatively slow photocurrent stability and a significant current attenuation within the 150 s. The integrated current density obtained by the external quantum efficiency (EQE) measurement is 22.3 and 23.1 mA/cm<sup>2</sup> for the pristine and 2% CTAB-added devices, respectively (Fig. 3e). The increased  $J_{sc}$  is in general agreement with the results of  $J$ – $V$  scanning and UV–Vis absorption. Finally, the PCE histogram distribution of 25 independent PSCs without or with different concentrations of CTAB doping is shown in Fig. 3f (each photovoltaic parameter distribution is displayed in Figure S7, Supporting Information); all devices show great reproducibility, and the 2% CTAB-doped samples exhibit the superior PCE distribution, meaning that 2% CTAB doping is the optimal concentration for defects passivation and efficiency improvement.

Electrochemical impedance spectroscopy (EIS) was measured to explore the transportation of charge and dynamic of carrier recombination in perovskite devices. The typical Nyquist plots with the corresponding equivalent electron circuit (the inset) were tested in the dark condition at  $V_{mpp}$ , as shown in Fig. 4a. As a general rule, there should be two arcs distribution in the higher and lower frequency, which represents the contact and recombination resistance in PSC, respectively [37–39]. However, in this work, only a large semicircle located in low frequency can be clearly observed in both samples. This is because the contact resistance is too small, which can be ignored compared to the recombination resistance. The EIS results based on reference and 2% CTAB additive devices are listed in Table S3. The 2% CTAB-added sample shows a smaller  $R_s$  (19.10  $\Omega$ ) and larger  $R_{rec}$  (4392  $\Omega$ ) comparing with the pristine ( $R_s = 21.36 \Omega$ ,  $R_{rec} = 2659 \Omega$ ), which indicated that the defects related with the nonradiative recombination could be efficiently passivated by CTAB.

The relationship between  $V_{oc}$  and various light intensity can be another convictive evidence for elucidating the recombination mechanism in PSCs [40, 41]. Two linear curves obtained by plotting  $V_{oc}$  versus logarithm light intensity with a slope of  $nkT/q$  are shown in Fig. 4b, where  $k$  is the Boltzmann constant,  $T$  is the absolute temperature, and  $q$  is the elementary charge [42]. Here, the fitted slope of the control and 2% CTAB added devices were 1.13 and 1.08  $kT/q$ , respectively. According to previous report, the slope is proportional to the density of trap states (the lower slope values indicated fewer traps) [43–45], which implied that we inhibited the trap states and decreased the charge recombination in PSCs by 2% CTAB doping. To further quantitatively

verify the variation of trap density after CTAB doping, we characterized the dark  $J-V$  characteristic of an electron-only device with the structure of glass/ITO/SnO<sub>2</sub>/perovskite/PCBM/Au, as Fig. 4c shows. The electron trap-state density can be expressed as  $V_{TEL}$  (trap-filled limited voltage), the kink point between linear ohmic response and nonlinear trap-filled response region, which indicates that injected carriers filled the traps. The trap-state density can be calculated by the following equation [46, 47]:

$$N_{trap} = \frac{2\epsilon_0\epsilon V_{TFL}}{eL^2}$$

where  $\epsilon_0$  is the vacuum permittivity,  $\epsilon$  is the relative dielectric constant of Cs<sub>0.05</sub>(FA<sub>0.85</sub>MA<sub>0.1</sub>)Pb(I<sub>0.85</sub>Br<sub>0.15</sub>)<sub>3</sub> (about 62.23 [48]),  $e$  is the elemental charge, and  $L$  is the thickness of the perovskite film. The  $V_{TEL}$  values of pristine and 2% CTAB-added perovskite film were 0.84 and 0.78V, respectively. Accordingly, the trap-state density reduced from original  $3.61 \times 10^{16}$  to  $3.27 \times 10^{16} \text{ cm}^{-3}$ . It is supported that the ion-induced trap states in perovskite film easily produced during the annealing process can be effectively passivated by CTAB doping [18], which is virtually identical to the above mentioned. We also noticed that CTAB has been applied to different systems in different ways to passivate the defects in perovskite solar cells or photodetectors [49–51]. However, in this paper, as a dopant, CTAB was first introduced into the precursor solution of ternary cation mixed halide perovskite solar cells, which exhibit superior photoelectric conversion efficiency, stability and commercial potential. By directly involving in the crystallization process of perovskite, CTAB can more simply and effectively reduce various ion defects in the process of film formation.

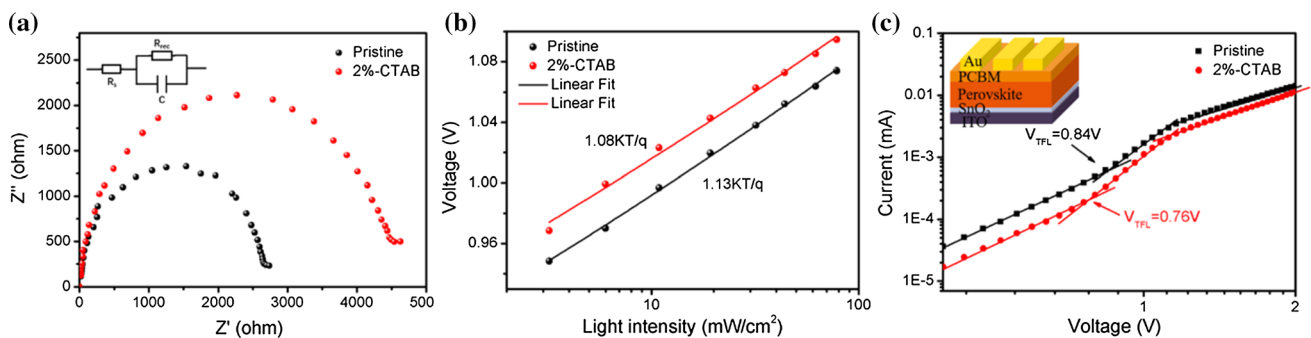


**Figure 4** a Nyquist plots of PSCs for pristine and CTAB doped with an inset equivalent circuit model. b Light intensity dependence of  $V_{oc}$  for PSCs based on pristine and CTAB-added

perovskite. c Dark  $J-V$  curves for electron-only devices with different perovskite layers; inset shows the structure of electron-only device.



Like Pandora's box, moisture can have a severe effect on efficiency of the PSCs and accelerate film decomposition. Figure 5a and Figure S8 show the water contact angle of the perovskite films without/with different concentrations of CTAB doping. It is obvious that the water droplet contact angle continuously increases as the amount of CTAB adding, which resulted from the long alkyl chain in CTAB molecule, can effectively improve the hydrophobicity of the perovskite film. As another important index to evaluate the performance of the PSCs, the stability under different ambient pressure is not negligible. The devices (unsealed) with and without CTAB doped were stored in glove box and continuously monitored the photovoltaic performance for 2000 h. As shown in Fig. 5b, the CTAB-added sample retained 94.3% of the initial efficiency, while the control device decreased to 86.7% of the initial efficiency under the same condition. The lower efficiency deficit implied that the CTAB-doped PSCs suffered from fewer defects destruction, exhibiting more superior stability. Humidity stability is another important component that is needed to be consideration. Hence, we put the unsealed PSCs (both control and 2% CTAB doped) in a humidity control box with relative humidity (RH) of 65% in air atmosphere. As illustrated in Fig. 5c, the efficiency of the 2% CTAB-doped device still maintains 73.5% of the initial efficiency, while the control device only reserves 30.1%

of the initial efficiency. The greatly enhanced humidity stability can be explained by the increased water contact angle, indicating that the long alkyl chain in CTAB molecule acts as a protective screen above the perovskite crystal blocking the grievous injury resulted from water. The improved stability and water resistance further demonstrated the excellent ability in defects passivation and moisture penetration protection of the CTAB doped in PSCs.

Combining the above results, CTAB as an additive in perovskite layer can passivate the defects and improve the photovoltaic performance of the devices. The passivation mechanism is shown in Fig. 6, and it can be interpreted as that:

1. The perovskite layer prepared by the sol-gel method will inevitably evolve some defects during the annealing process, such as vacancies and antisite. The incorporation of Br and quaternary cetyl tertiary ammonium cations ( $\text{CTA}^+$ ) of CTAB in perovskite film can remedy the halogen and cation defects and improve the performance of the PSCs.
2. The long alkyl chain has a better hydrophobic than methyl ammonium (MA) or formamidinium (FA). Therefore, an appropriate amount of hexadecyl long-chain group is introduced to increase the water contact angle of the perovskite film, which enhances the hydrophobic property of the

**Figure 5** a Water contact angles of perovskite film with and without CTAB additive. b The stability test of the corresponding unsealed PSCs under  $\text{N}_2$  atmosphere. c Humidity stability test of the PSCs without encapsulation stored in air and 65% relative humidity.

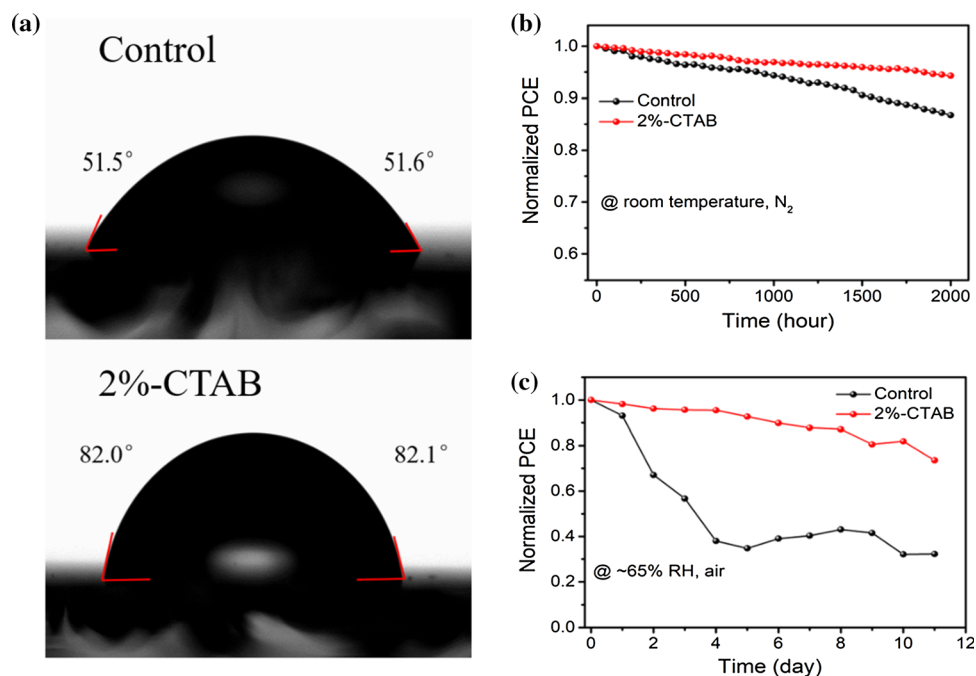
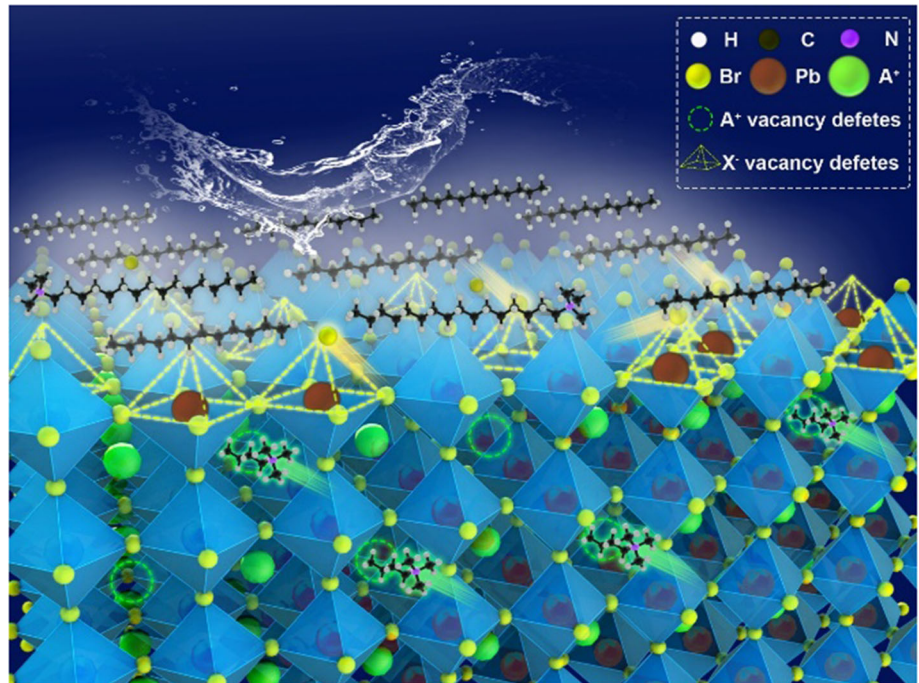




**Figure 6** The mechanism image of CTAB defects passivation of perovskite layers induced by A-site or X-site vacancies and the hydrophobic properties of the long alkyl chains in CTAB.



material and thus improves the stability of the devices in the high humidity air condition.

- Excessive CTAB additive inhibited the transformation of  $\text{PbI}_2$  to perovskite phase, reducing the crystallinity and grain size of the perovskite film. The greatly increased contact angle (3% CTAB) is harmful to the deposition of the HTL and impair the carrier transportation between perovskite layer and CTL. As a result, the performance of the devices degraded significantly.

## Conclusion

In summary, we took an efficient approach through adding the appropriate amount of CTAB in perovskite precursor solution to both passivate the ionic defects in perovskite film and block the water penetration, improving the efficiency and stability of the PSCs. The CTAB-doped perovskite film reveals the decreased imperfection and improved water resistance. This is due to the synergistic effect of multifunction molecule including quaternary ammonium cation, halogen bromide and long alkyl chain realizing the defects passivation and perovskite grain protection. As such, an exciting enhancement in average PCE from the original 17.85–19.54% has been

achieved. Simultaneously, the environment and moisture stability of the CTAB-doped PSCs have been improved significantly. This work proposes a reference for addressing the multiple issues in perovskite solar cells by multifunctional molecules synergistic working, which are critical for promoting the development of PSCs industrialization as soon as possible.

## Acknowledgements

The research was funded by the Youth Science and Technology Innovation Team Project of SWPU (No. 2019CXTD04) and Important Master Innovation Project of SWPU (2019cxzd014).

## Compliance with ethical standards

**Conflict of interest** There are no conflicts of interest to declare.

**Electronic supplementary material:** The online version of this article (<https://doi.org/10.1007/s10853-020-05059-7>) contains supplementary material, which is available to authorized users.

## References

- [1] McMeekin DP, Sadoughi G, Rehman W, Eperon GE, Saliba M, Hoerantner MT, Haghighirad A, Sakai N, Korte L, Rech B, Johnston MB, Herz LM, Snaith HJ (2016) A mixed-cation lead mixed-halide perovskite absorber for tandem solar cells. *Science* 351(6269):151–155. <https://doi.org/10.1126/science.aad5845>
- [2] Sutton RJ, Eperon GE, Miranda L, Parrott ES, Kamino BA, Patel JB, Horantner MT, Johnston MB, Haghighirad AA, Moore DT, Snaith HJ (2016) Bandgap-tunable cesium lead halide perovskites with high thermal stability for efficient solar cells. *Adv Energy Mater* 6(8):1502458. <https://doi.org/10.1002/aenm.201502458>
- [3] Xing G, Mathews N, Sun S, Lim SS, Lam YM, Graetzel M, Mhaisalkar S, Sum TC (2013) Long-range balanced electron- and hole-transport lengths in organic-inorganic  $\text{CH}_3\text{NH}_3\text{PbI}_3$ . *Science* 342(6156):344–347. <https://doi.org/10.1126/science.1243167>
- [4] Stranks SD, Eperon GE, Grancini G, Menelaou C, Alcocer MJP, Leijtens T, Herz LM, Petrozza A, Snaith HJ (2013) Electron-hole diffusion lengths exceeding 1 micrometer in an organometal trihalide perovskite absorber. *Science* 342(6156):341–344. <https://doi.org/10.1126/science.1243982>
- [5] Kojima A, Teshima K, Shirai Y, Miyasaka T (2009) Organometal halide perovskites as visible-light sensitizers for photovoltaic cells. *J Am Chem Soc* 131(17):6050–6051. <https://doi.org/10.1021/ja809598r>
- [6] NREL (2019) NREL Best Research-Cell Efficiencies, <https://www.nrel.gov/pv/assets/images/efficiency-chart.png>
- [7] Nagabhushana GP, Shivaramaiah R, Navrotsky A (2016) Direct calorimetric verification of thermodynamic instability of lead halide hybrid perovskites. *Proc Natl Acad Sci USA* 113(28):7717–7721. <https://doi.org/10.1073/pnas.1607850113>
- [8] Ivanov IL, Steparuk AS, Bolyachkina MS, Tsvetkov DS, Safronov AP, Zuev AY (2018) Thermodynamics of formation of hybrid perovskite-type methylammonium lead halides. *J Chem Thermodyn* 116:253–258. <https://doi.org/10.1016/j.jct.2017.09.026>
- [9] deQuilettes DW, Vorpahl SM, Stranks SD, Nagaoka H, Eperon GE, Ziffer ME, Snaith HJ, Ginger DS (2015) Impact of microstructure on local carrier lifetime in perovskite solar cells. *Science* 348(6235):683–686. <https://doi.org/10.1126/science.aaa5333>
- [10] Zhu K, Miyasaka T, Kim JY, Mora-Sero I (2015) Trend of perovskite solar cells: dig deeper to build higher. *J Phys Chem Lett* 6(12):2315–2317. <https://doi.org/10.1021/acs.jpclett.5b01033>
- [11] Simpson MJ, Doughty B, Yang B, Xiao K, Ma Y-Z (2016) Imaging electronic trap states in perovskite thin films with combined fluorescence and femtosecond transient absorption microscopy. *J Phys Chem Lett* 7(9):1725–1731. <https://doi.org/10.1021/acs.jpclett.6b00715>
- [12] Wang Q, Chen B, Liu Y, Deng Y, Bai Y, Dong Q, Huang J (2017) Scaling behavior of moisture-induced grain degradation in polycrystalline hybrid perovskite thin films. *Energy Environ Sci* 10(2):516–522. <https://doi.org/10.1039/c6ee02941h>
- [13] Shao Y, Fang Y, Li T, Wang Q, Dong Q, Deng Y, Yuan Y, Wei H, Wang M, Gruverman A, Shialda J, Huang J (2016) Grain boundary dominated ion migration in polycrystalline organic-inorganic halide perovskite films. *Energy Environ Sci* 9(5):1752–1759. <https://doi.org/10.1039/c6ee00413j>
- [14] Si H, Liao Q, Kang Z, Ou Y, Meng JJ, Liu Y, Zhang Z, Zhang Y (2017) Deciphering the  $\text{NH}_4\text{PBI}_3$  intermediate phase for simultaneous improvement on nucleation and crystal growth of perovskite. *Adv Funct Mater* 27(30):1701804. <https://doi.org/10.1002/adfm.201701804>
- [15] Zheng X, Chen B, Dai J, Fang Y, Bai Y, Lin Y, Wei H, Zeng XC, Huang J (2017) Defect passivation in hybrid perovskite solar cells using quaternary ammonium halide anions and cations. *Nature Energy* 2(7):Unsp 17102. <https://doi.org/10.1038/nenergy.2017.102>
- [16] Yang Y, Feng S, Li M, Li F, Zhang C, Han Y, Li L, Yuan J, Cao L, Wang Z, Sun B, Gao X (2018) Enormously improved  $\text{CH}_3\text{NH}_3\text{PbI}_3$  film surface for environmentally stable planar perovskite solar cells with PCE exceeding 19.9%. *Nano Energy* 48:10–19. <https://doi.org/10.1016/j.nanoen.2018.03.046>
- [17] Zhao Y, Wei J, Li H, Yan Y, Zhou W, Yu D, Zhao Q (2016) A polymer scaffold for self-healing perovskite solar cells. *Nat Commun* 7:10228. <https://doi.org/10.1038/ncomms10228>
- [18] Noel NK, Abate A, Stranks SD, Parrott ES, Burlakov VM, Goriely A, Snaith HJ (2014) Enhanced photoluminescence and solar cell performance via lewis base passivation of organic inorganic lead halide perovskites. *ACS Nano* 8(10):9815–9821. <https://doi.org/10.1021/nn5036476>
- [19] Tu Y, Yang X, Su R, Luo D, Cao Y, Zhao L, Liu T, Yang W, Zhang Y, Xu Z, Liu Q, Wu J, Gong Q, Mo F, Zhu R (2018) Diboron-assisted interfacial defect control strategy for highly efficient planar perovskite solar cells. *Adv Mater* 30(49):1805085. <https://doi.org/10.1002/adma.201805085>
- [20] Wen TY, Yang S, Liu PF, Tang LJ, Qiao HW, Chen X, Yang XH, Hou Y, Yang HG (2018) Surface electronic modification of perovskite thin film with water-resistant electron delocalized molecules for stable and efficient photovoltaics. *Adv*

- Energy Mater 8(13):1703143. <https://doi.org/10.1002/aenm.201703143>
- [21] Zhang F, Shi W, Luo J, Pellet N, Yi C, Li X, Zhao X, Dennis TJS, Li X, Wang S, Xiao Y, Zakeeruddin SM, Bi D, Graetzel M (2017) Isomer-pure Bis-PCBM-assisted crystal engineering of perovskite solar cells showing excellent efficiency and stability. *Adv Mater* 29(17):1606806. <https://doi.org/10.1002/adma.201606806>
- [22] Li H, Wu G, Li W, Zhang Y, Liu Z, Wang D, Liu S (2019) Additive engineering to grow micron-sized grains for stable high efficiency perovskite solar cells. *Adv Sci* 6(18):1901241. <https://doi.org/10.1002/advs.201901241>
- [23] Wei F, Jiao B, Dong H, Xu J, Lei T, Zhang J, Yu Y, Ma L, Wang D, Chen J, Hou X, Wu Z (2019) Bifunctional pi-conjugated ligand assisted stable and efficient perovskite solar cell fabrication via interfacial stitching. *J Mater Chem A* 7(27):16533–16540. <https://doi.org/10.1039/c9ta03898a>
- [24] Ding S, Li S, Sun Q, Wu Y, Liu Y, Li Z, Cui Y, Wang H, Hao Y, Wu Y (2019) Enhanced performance of perovskite solar cells by the incorporation of the luminescent small molecule DBP: perovskite absorption spectrum modification and interface engineering. *J Mater Chem C* 7(19):5686–5694. <https://doi.org/10.1039/c9tc00064j>
- [25] Abate A, Saliba M, Hollman DJ, Stranks SD, Wojciechowski K, Avolio R, Grancini G, Petrozza A, Snaith HJ (2014) Supramolecular halogen bond passivation of organic-inorganic halide perovskite solar cells. *Nano Lett* 14(6):3247–3254. <https://doi.org/10.1021/nl500627x>
- [26] Wang B, Wu F, Bi S, Zhou J, Wang J, Leng X, Zhang D, Meng R, Xue B, Zong C, Zhu L, Zhang Y, Zhou H (2019) A polyaspartic acid sodium interfacial layer enhances surface trap passivation in perovskite solar cells. *J Mater Chem A* 7(41):23895–23903. <https://doi.org/10.1039/c9ta01947b>
- [27] Bi D, Yi C, Luo J, Decoppet J-D, Zhang F, Zakeeruddin SM, Li X, Hagfeldt A, Gratzel M (2016) Polymer-templated nucleation and crystal growth of perovskite films for solar cells with efficiency greater than 21%. *Nature Energy* 1:16142. <https://doi.org/10.1038/nenergy.2016.142>
- [28] Chen Q, Zhou H, Song T-B, Luo S, Hong Z, Duan H-S, Dou L, Liu Y, Yang Y (2014) Controllable self-induced passivation of hybrid lead iodide perovskites toward high performance solar cells. *Nano Lett* 14(7):4158–4163. <https://doi.org/10.1021/nl501838y>
- [29] Jacobsson TJ, Correa-Baena J-P, Anaraki EH, Philippe B, Stranks SD, Bouduban MEF, Tress W, Schenk K, Teuscher J, Moser J-E, Rensmo H, Hagfeldt A (2016) Unreacted PbI<sub>2</sub> as a double-edged sword for enhancing the performance of perovskite solar cells. *J Am Chem Soc* 138(32):10331–10343. <https://doi.org/10.1021/jacs.6b06320>
- [30] Flinn PA, Chiang C (1990) X-ray diffraction determination of the effect of various passivations on stress in metal films and patterned lines. *J Appl Phys* 67:2927–2931
- [31] Zhang H, Wang H, Chen W, Jen AKY (2017) CuGaO<sub>2</sub>: a promising inorganic hole-transporting material for highly efficient and stable perovskite solar cells. *Adv Mater* 29(8):Unsp 1604984. <https://doi.org/10.1002/adma.201604984>
- [32] Wu W-Q, Yang Z, Rudd PN, Shao Y, Dai X, Wei H, Zhao J, Fang Y, Wang Q, Liu Y, Deng Y, Xiao X, Feng Y, Huang J (2019) Bilateral alkylamine for suppressing charge recombination and improving stability in blade-coated perovskite solar cells. *Science Advances* 5(3):eaav8925. <https://doi.org/10.1126/sciadv.aav8925>
- [33] Chen B, Yang M, Zheng X, Wu C, Li W, Yan Y, Bisquert J, Garcia-Belmonte G, Zhu K, Priya S (2015) Impact of capacitive effect and ion migration on the hysteretic behavior of perovskite solar cells. *J Phys Chem Lett* 6(23):4693–4700. <https://doi.org/10.1021/acs.jpcclett.5b02229>
- [34] Kong D-H, Park N-G (2019) On the current-voltage hysteresis in perovskite solar cells: dependence on perovskite composition and methods to remove hysteresis. *Adv Mater* 31(34):1805214. <https://doi.org/10.1002/adma.201805214>
- [35] The D, Wu Y, Shen H, Peng J, Fu X, Jacobs D, Wang E-C, Kho TC, Fong KC, Stocks M, Franklin E, Blakers A, Zin N, McIntosh K, Li W, Cheng Y-B, White TP, Weber K, Catchpole K (2017) Rubidium multication perovskite with optimized bandgap for perovskite-silicon tandem with over 26% efficiency. *Adv Energy Mater* 7(14):1700228. <https://doi.org/10.1002/aenm.201700228>
- [36] Chen B, Yang M, Priya S, Zhu K (2016) Origin of J-V hysteresis in perovskite solar cells. *J Phys Chem Lett* 7(5):905–917. <https://doi.org/10.1021/acs.jpcclett.6b00215>
- [37] Chaudhary B, Kulkarni A, Jena AK, Ikegami M, Udagawa Y, Kunugita H, Ema K, Miyasaka T (2017) Poly(4-Vinylpyridine)-based interfacial passivation to enhance voltage and moisture stability of lead halide perovskite solar cells. *Chemosuschem* 10(11):2473–2479. <https://doi.org/10.1002/cssc.201700271>
- [38] Qin F, Tong J, Ge R, Luo B, Jiang F, Liu T, Jiang Y, Xu Z, Mao L, Meng W, Xiong S, Li Z, Li L, Zhou Y (2016) Indium tin oxide (ITO)-free, top-illuminated, flexible perovskite solar cells. *J Mater Chem A* 4(36):14017–14024. <https://doi.org/10.1039/c6ta06657g>
- [39] Yang D, Yang R, Zhang J, Yang Z, Liu S, Li C (2015) High efficiency flexible perovskite solar cells using superior low temperature TiO<sub>2</sub>. *Energy Environ Sci* 8(11):3208–3214. <https://doi.org/10.1039/c5ee02155c>

- [40] Liu X, Wang H-Q, Li Y, Gui Z, Ming S, Usman K, Zhang W, Fang J (2017) Regular organic solar cells with efficiency over 10% and promoted stability by ligand- and thermal annealing-free Al-doped ZnO cathode interlayer. *Adv Sci* 4(8):1700053. <https://doi.org/10.1002/advs.201700053>
- [41] Fu S, Li X, Wan L, Wu Y, Zhang W, Wang Y, Bao Q, Fang J (2019) Efficient passivation with lead Pyridine-2-Carboxylic for high-performance and stable perovskite solar cells. *Adv Energy Mater* 9(35):1901852. <https://doi.org/10.1002/aenm.201901852>
- [42] Peng W, Wang L, Murali B, Ho K-T, Bera A, Cho N, Kang C-F, Burlakov VM, Pan J, Sinatra L, Ma C, Xu W, Shi D, Alarousu E, Goriely A, He J-H, Mohammed OF, Wu T, Bakr OM (2016) Solution-grown monocrystalline hybrid perovskite films for hole-transporter-free solar cells. *Adv Mater* 28(17):3383–3390. <https://doi.org/10.1002/adma.201506292>
- [43] Mandoc MM, Veurman W, Koster LJA, de Boer B, Blom PWM (2007) Origin of the reduced fill factor and photocurrent in MDMO-PPV:PCNEPV all-polymer solar cells. *Adv Funct Mater* 17(13):2167–2173
- [44] Mandoc MM, Kooistra FB, Hummelen JC, de Boer B, Blom WM (2007) Effect of traps on the performance of bulk heterojunction organic solar cells. *Appl Phys Lett* 91:263505
- [45] Sherkar TS, Momblona C, Gil-Escrig L, Avila J, Sessolo M, Bolink HJ, Koster LJA (2017) Recombination in perovskite solar cells: significance of grain boundaries interface traps, and defect ions. *ACS Energy Lett* 2(5):1214–1222. <https://doi.org/10.1021/acseenergylett.7b00236>
- [46] Shi D, Adinolfi V, Comin R, Yuan M, Alarousu E, Buin A, Chen Y, Hoogland S, Rothenberger A, Katsiev K, Losovsky Y, Zhang X, Dowben PA, Mohammed OF, Sargent EH, Bakr OM (2015) Low trap-state density and long carrier diffusion in organolead trihalide perovskite single crystals. *Science* 347(6221):519–522. <https://doi.org/10.1126/science.aaa2725>
- [47] Bube RH (1962) Trap density determination by space-charge-limited currents. *J Appl Phys* 33(5):1733–1737
- [48] Liu Y, Sun J, Yang Z, Yang D, Ren X, Xu H, Yang Z, Liu S (2016) 20-mm-large single-crystalline formamidinium-perovskite wafer for mass production of integrated photodetectors. *Adv Opt Mater* 4(11):1829–1837. <https://doi.org/10.1002/adom.201600327>
- [49] Ghorai A, Midya A, Ray SK (2019) Surfactant-induced anion exchange and morphological evolution for composition-controlled caesium lead halide perovskites with tunable optical properties. *ACS Omega* 4(7):12948–12954. <https://doi.org/10.1021/acsomega.9b00829>
- [50] Cai Y, Wang L, Zhou T, Zheng P, Li Y, Xie R-J (2018) Improved stability of CsPbBr<sub>3</sub> perovskite quantum dots achieved by suppressing interligand proton transfer and applying a polystyrene coating. *Nanoscale* 10(45):21441–21450. <https://doi.org/10.1039/c8nr06607h>
- [51] Wang S, Zhu Y, Wang C, Ma R (2019) Interface modification by a multifunctional ammonium salt for high performance and stable planar perovskite solar cells. *J Mater Chem A* 7(19):11867–11876. <https://doi.org/10.1039/c9ta02631b>

**Publisher's Note** Springer Nature remains neutral with regard to jurisdictional claims in published maps and institutional affiliations.